Applied Geography 111 (2019) 102077

Contents lists available at ScienceDirect

Applied Geography

journal homepage: www.elsevier.com/locate/apgeog

# Monitoring land-cover and land-use dynamics in Fanjingshan National Nature Reserve

Yu Hsin Tsai[a,*], Douglas Stow[a], Li An[a], Hsiang Ling Chen[b,d], Rebecca Lewison[d], Lei Shi[c]

[a] Department of Geography, San Diego State University, USA
[b] Department of Forestry, National Chung Hsing University, Taiwan
[c] Fanjingshan National Nature Reserve Administration, China
[d] Department of Biology, San Diego State University, USA

ARTICLE INFO

*Keywords:*
Land-cover and land-use change
Payment for ecosystem services
Protected area
Landsat
China
Google earth engine

ABSTRACT

Fanjingshan National Nature Reserve (FNNR) in China is a biodiversity hotspot that is part of a larger, multi-use landscape where tourism, farming, grazing, and other land uses occur. Payment for ecosystem services (PES) programs that encourage afforestation on farmlands may be important drivers of land-cover and land-use change in the region that surrounds FNNR. Our objective is to monitor and examine vegetation and land-use changes, including PES-related afforestation, between 1989 and 2017. We utilize several image processing techniques, such as illumination normalization approaches to suppress terrain effects, and multi-seasonal image compositing to minimize persistent cloud cover. Ancillary data were also incorporated to generate reliable vegetation and land-use change information. A random forest machine learning image classification routine is implemented through the cloud-based Google Earth Engine platform and refined using optimal classifier parameter tuning. Land-use transitions are identified and mapped with the implementation of stable training sites, discrete image classification, and logical land-use transition rules. Accuracy assessment results indicate our change detection workflow provides a reliable methodology to remotely monitor long-term forest cover and land-use changes in this mountainous, forested, and cloud prevalent region. We quantify the area of new built development and afforestation land and found that most of the land transitions took place in reserve buffer and its adjacent environs. For example, less than 2 $km^2$ of new built was identified within the reserve boundary compared to 25 $km^2$ for the entire study area between 1995 and 2016. We also shed light on the strengths and weaknesses of using Google Earth Engine for land-cover and land-use change studies. This efficient and open-access technique is important not only for assessing environmental changes and PES efficacy, but also for evaluating other conservation policies elsewhere.

## 1. Introduction

Frequent anthropogenic disturbances can lead to land-cover and land-use change (LCLUC) and cause ecosystems to degrade quickly, even within designated protected areas (Liu et al., 2001). The most feasible and efficient means for monitoring widespread and accelerated LCLUC is through satellite remote sensing. Landsat satellite systems provide a long-term and freely-available image archive which is ideal for LCLUC monitoring applications. Landsat imagery has the potential temporal frequency of every 16 days and a moderate (30 m) spatial resolution. Reliable change analyses can be achieved with surface reflectance products (Hall, Strebel, Nickson, & Goetz, 1991; Moran, Jackson, Slater, & Teillet, 1992). Surface reflectance products for Landsat 4 to 7 and Landsat 8 data are processed through automatic algorithms of the Landsat Ecosystem Disturbance Adaptive Processing System (LEDAPS; Masek, 2006) and Landsat Surface Reflectance Code (LaSRC; Vermote, Justice, Claverie, & Franch, 2016) respectively. By converting digital numbers to surface reflectance values, most atmospheric and solar illumination effects are corrected. These corrections enable multi-temporal Landsat images to be more comparable over time.

Different image classification and change identification techniques have been implemented for semi-automated land change studies. A conventional maximum likelihood classifier combined with stable training sites was used to classify nine Landsat image dates for a cloud-prone study area (Stow, Shih, & Coulter, 2014). The technique was deemed effective for long-term LCLUC monitoring. Machine learning type image classifiers were tested by Schneider (2012) with dense

* Corresponding author.
*E-mail address:* cindyxtsai@gmail.com (Y.H. Tsai).

https://doi.org/10.1016/j.apgeog.2019.102077
Received 23 August 2018; Received in revised form 29 June 2019; Accepted 27 August 2019

Landsat image stacks and training sites of stable and changed features. Among the tested image classifiers, random forest (RF) and support vector machine (SVM) classifiers yielded high accuracies; the RF classifier was found to handle missing image data best. Although machine learning type image classifiers may require larger training samples (Kotsiantis, Zaharakis, & Pintelas, 2007), the RF image classifier was determined by Rodriguez-Galiano, Ghimire, Rogan, Chica-Olmo, and Rigol-Sanchez (2012) to be less sensitive to small training sample sizes. To quantify land-use changes and retain the transition classes, a post-classification map comparison step was demonstrated by Yuan, Sawaya, Loeffelholz, and Bauer (2005) to be effective.

China has two of the largest payment for ecosystem services (PES) programs in the world (Liu, Li, Ouyang, Tam, & Chen, 2008), which aim to increase forest cover and reduce soil erosion and flooding following the long history of deforestation since the 1960s (Harkness, 1998) and major flooding in 1998 (Uchida, Xu, & Rozelle, 2005). The two main PES programs in China are commonly known as the National Forest Conservation Program (NFCP) and Grain to Green Program (GTGP). The NFCP was implemented in 1998, and the GTGP went into effect in 1999. Under the NFCP regulations, timber harvest would be reduced or even eliminated from natural forests (Liu et al., 2008). The goals are for plantation forests to become the main source of timber harvesting, while natural forests are restored by banning firewood and resource collection. The GTGP policy has a stronger focus on reducing soil erosion by afforestation on sloped land (Uchida et al., 2005). Strategies include afforestation on barren land, and converting farmland located on steep slopes (i.e., steeper than 25° in southern China; Xu, Tao, Xu, & Bennett, 2010) to ecological or economic trees. The Chinese government provides payment incentives for both programs. Farmers who enroll in GTGP receive financial and crop compensations, as well as seedlings for afforestation. The participants of NFCP receive financial support in exchange for forest protection (e.g. patrol and fire watch) and not utilizing forest resources.

Several studies have demonstrated the utility of remote sensing to monitoring afforestation in China, though most of them focused on the drier, northern portion of the country. Zhou and Van Rompaey (2009) utilized SPOT satellite time series images and derived vegetation indices to monitor GTGP in Shaanxi. Significant vegetation cover increase was mapped for the drier portion of their study area, while no vegetation change was detected in the humid and irrigated region. Using Landsat images, Zhou, Zhao, and Zhu (2012) quantified land transitions from agriculture and grassland to afforested land in the semi-arid Loess Plateau area. Their results showed rapid afforestation activity occurred after GTGP implementation and a more fragmented landscape was observed. Landsat time-series images were used to map deforestation and afforestation by Liu et al. (2013) for a 38-year period south of Mongolia. Their highly accurate (89%) results indicated large-scale afforestation activity could be monitored using remote sensing techniques. Spatially extensive quantitative data about distribution and effectiveness of PES activities in the more humid, southern portion of China remain minimal.

Located in southeastern China, Fanjingshan National Nature Reserve (FNNR) is on the UNESCO World Heritage List because of its high fauna and flora biodiversity, with over 100 endemic species found in the reserve. Roughly 13,000 people live a subsistence life style within the protected area, with a total of 21,000 population within or near the region surrounding FNNR (Global Environmental Facility Project Team, 2004). Human land-use activities such as farming, grazing, and resource gathering take place within or near the reserve (Wandersee, 2013). FNNR has experienced rapid and complex land-use changes in recent years, due to changing demographic patterns, economic and tourism growth, and related development. In 2008, a gondola lift system was built to transport tourists from the east reserve entrance to the FNNR peak. An expanded road network that surrounds the reserve was completed in 2010 (Aitken, An, & Yang, 2019). PES programs have been implemented in the FNNR region for over 17 years. The last two decades have witnessed increasing outmigration from FNNR to cities as well as rapid initiation and expansion of local off-farm businesses, imposing substantial impacts on FNNR's land use and land cover. Given the wide-spread human activities and the resultant rapid land changes in this pristine, mountainous, and cloud-prone reserve, a closer examination of how to monitor LCLUC in an efficient and reliable manner is important for reserve management.

FNNR is a temperate, cloud-prone region with steep terrain and mixed forest cover types, which are great challenges when mapping and monitoring land surfaces using optical remote sensing approaches. Seasonal image composites have been shown to increase the separability of vegetation types and to minimize missing data due to cloud cover (Franco-Lopez, Ek, & Bauer, 2001; Rodriguez-Galiano et al., 2012). Shade and illumination normalization techniques (Tsai, Stow, Shi, Lewison, & An, 2016; Wu, 2004) and spectral vegetation index (SVI) products (Qi, Chehbouni, Huete, Kerr, & Sorooshian, 1994) have been demonstrated to suppress illumination, terrain, and soil reflectance influences. Ancillary data, such as elevation models, were found to improve vegetation classification accuracy (Belgiu & Drăguţ, 2016; Domaç & Süzen, 2006; Dorren, Maier, & Seijmonsbergen, 2003; Xie, Sha, & Yu, 2008). The combined usage of seasonal image composites, illumination normalization, SVIs, and ancillary data in a previous study mapping vegetation and land-use in FNNR yielded consistent mapping results with moderate accuracy (Tsai et al., 2018).

A software platform that has been instructive in efficient open-access image processing is Google Earth Engine (https://earthengine.google.com). Earth Engine is a cloud-based and open-access geospatial data analysis platform (Gorelick, 2017). It provides an image library that can be directly accessed through the JavaScript coding environment. The image library contains data from various sensors and satellite platforms, including almost the entire Landsat image archive and its surface reflectance products. The coding environment allows users to test and implement algorithms and interactively view results. Earth Engine also provides many machine learning type image classifiers for mapping applications. The efficiency of this platform has been demonstrated by Hansen et al. (2013), who generated global forest cover change products from over 650 thousand Landsat 7 scenes in just days. Johansen, Phinn, and Taylor (2015) achieved high mapping accuracies using machine learning image classifiers with Landsat images on Google Earth Engine in a study mapping woody vegetation change.

The primary objective of this study is to map, monitor, and quantify land-use transitions pertaining to afforestation and anthropogenic development for the FNNR and its environs. A secondary objective is to assess the utility of monitoring land-use dynamics in the cloud prone and steep terrain study area through Landsat satellite images and Google Earth Engine deploying a workflow previously developed by Tsai et al. (2018). Our hypothesis is that machine learning classification of multi-temporal Landsat images are sufficiently accurate to effectively monitor land-use changes in the FNNR region. We map vegetation and land-use types with images captured before and after the PES program implementation in the FNNR region. Techniques such as shade and illumination normalization, and multi-seasonal Landsat image stacks are employed to account for terrain-illumination effects and persistent cloud cover in the study area. Stable training sites are utilized to train a random forest machine learning image classifier to generate vegetation and land-use maps for four periods from 1989 to 2017. Land-use transitions focusing on afforestation and new developments are subsequently mapped. Land-transition maps are examined in conjunction with high spatial resolution satellite imagery to identify corresponding land-use changes.

## 2. Study area and data

FNNR in Guizhou province (27.92 N, 108.70 E) was listed as one of the 25 global biodiversity hotspots (Myers, Mittermeier, Mittermeier, Da Fonseca, & Kent, 2000). Established in 1978, there are over 5000

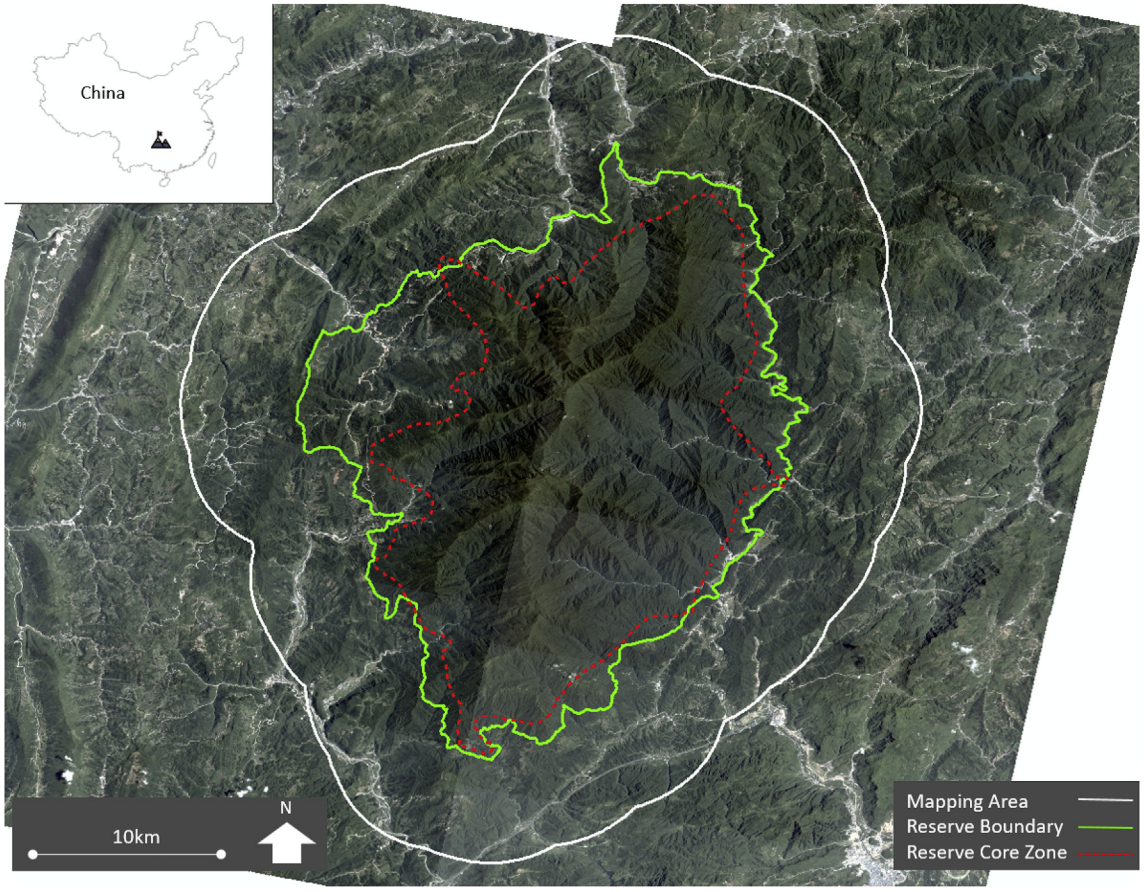


**Fig. 1.** Fanjingshan National Nature Reserve in southeastern China. The reserve boundary is outlined in green, while the reserve core zone in dotted red is slightly smaller. The mapping area (including a 6 km buffer from the reserve boundary) for this study is outlined in white. The backdrop image is a true-color satellite image mosaic collected by Planet Team in July 2017. The mosaicked Planet image exhibits bidirectional reflectance effects but is suitable for visual interpretation. (For interpretation of the references to color in this figure legend, the reader is referred to the Web version of this article.)

species of plants and animals identified in the reserve. The reserve can be divided into core and buffer zones, totaling about 419 $km^2$ in size (Yang, Lei, & Yang, 2002). Fig. 1 shows our study/mapping area, which includes the reserve core area, the buffer zone, and an area that extends outward by 6 km from the buffer zone to incorporate nearby villages. Forest cover in the reserve core is mostly undisturbed primary forests. The forest composition is complex and mixed. For mapping purposes, we generalize the forest community types based on dominant species into five types: deciduous, evergreen broadleaf, mixed deciduous and evergreen, bamboo, and conifer. Villages and agriculture are found in the surrounding hinterlands of the reserve. These surrounding areas also contain mixed and secondary forests, as well as afforested.

Vegetation from PES programs. Both NFCP and GTGP PES programs are implemented in the FNNR region. The implementation started around year 2001. An estimated 9000 mu (6 $km^2$) of farmland was enrolled in GTGP for afforestation during 2001–2008 (Wandersee, 2013). About 3 $km^2$ of land in the reserve were designated as GTGP lands based on a hand-digitized layer created by the reserve staff. In most cases, participants plant pine or fir trees in a mono-crop style. In some occasions, bamboo and economical plants such as tea and fruit trees are also planted.

Available Landsat surface reflectance images that cover the FNNR region (World Reference System 2 path 126, row 41) were identified for the following study periods: Time 1 circa 1989, Time 2 circa 1995, Time 3 circa 2010, and Time 4 circa 2016. Table 1 provides information on specific image dates and number of images used. The four study periods were selected to coincide with and based on (1) the earliest available Landsat data after reserve establishment, (2) prior to and after the GTGP implementation in the region in 2001, and (3) the most up-to-date land-use and land-cover. A four- and six-year image cycle was found to be appropriate to monitor anthropogenic-related vegetation changes (Coppin & Bauer, 1995), and a ten-year interval was found sufficient to transition from successional vegetation to forest (Park, Houghton, Hicks, & Peterson, 1983).

**Table 1**
Image dates and number of images associated with the study periods for this study.

| Study Period | Sensor | Seasonal Composite Images | Number of Images |
|---|---|---|---|
| Circa 1989 | Landsat 5 | 1989–1990 | 12 images |
| Circa 1995 | Landsat 5 | 1995–1996 | 12 images |
| Circa 2010 | Landsat 5 | 2010–2011 | 11 images |
| Circa 2016 | Landsat 8 | 2016–2017 | 17 images |

A digital elevation layer from the Shuttle Radar Topography Mission (SRTM) was incorporated in the classification workflow. C-band and X-band data were collected with different antenna panels for SRTM in the year 2000 (Farr, 2007). The C-band derived digital elevation model (DEM) has near-global coverage and was processed by NASA JPL. The one arc-second (roughly 30 m) spatial resolution topographic data were released for public use in 2015.

Some high spatial resolution satellite imagery data were available for viewing, and were utilized during our analysis. Imagery data include true-color Pleiades images from 2013 to 2017 on Google Earth, and pan-sharpened QuickBird/GeoEye/WorldView-2 mosaic images from 2004 to 2012 available as Basemap in the ArcGIS software. Four-

band Planet images (red, green, blue, and near-infrared bands) were made available through its Education and Research Program (Planet Team, 2017). We generated two cloud-free mosaicked products from Summer 2016 and Summer 2017 for the FNNR study area. The mosaicked image set exhibits bidirectional effects, however it is suitable for our visual interpretation purposes.

## 3. Methods

Vegetation and land-use types were mapped for each of four study periods and the resultant maps were assessed for accuracy. Then land-transition maps were generated through post-classification map comparison to emphasize lands that underwent afforestation and development of new built land cover.

### 3.1. Classification feature input

All available Landsat surface reflectance images for each study period are listed in Table 1. Images for the same year were first compiled into seasonal composites. Based on capture dates, images were split into spring, summer, and fall season groups. The winter months (i.e., December through February) were excluded due to leaf-off conditions. A mean value composite image was generated for each season group before they were layerstacked for each study period. Several types of SVI image sets were derived for each season group and image date, for subsequent input to image classifiers. The indices were meant to enhance vegetation and soil moisture signature, and suppress terrain illumination differences. These included normalized difference vegetation index (NDVI; Carlson & Ripley, 1997), modified soil adjusted vegetation index (MSAVI; Qi et al., 1994), normalized difference blue and red (NDBR), normalized difference green and red (NDGR), normalized difference shortwave infrared and near infrared (NDII), and spectral variability vegetation index (SVVI; Coulter, 2016). NDVI is calculated as Equation (1):

$$\mathrm{NDVI} = \frac{\rho_{\mathrm{NIR}} - \rho_{\mathrm{red}}}{\rho_{\mathrm{NIR}} + \rho_{\mathrm{red}}} \quad (1)$$

and MSAVI is calculated as Equation (2):

$$\mathrm{MSAVI} = \frac{2\rho_{\mathrm{NIR}} + 1 - \sqrt{(2\rho_{\mathrm{NIR}} + 1)^2 - 8(\rho_{\mathrm{NIR}} - \rho_{\mathrm{red}})}}{2} \quad (2)$$

here $\rho_{\mathrm{NIR}}$ and $\rho_{\mathrm{red}}$ in Equations (1) and (2) represent the near infrared and red reflectance values for a given pixel. NDBR, NDGR, and NDII are calculated as the form of NDVI in Equation (1), using blue and red bands for NDBR, green and red bands for NDGR, and infrared bands (NIR and SWIR) for NDII. SVVI is calculated as the pixel-wise difference between standard deviation (SD) of all Landsat bands (excluding thermal) and SD of all three infrared bands, as shown in Equation (3):

$$\mathrm{SVVI} = SD(\rho_{\text{all bands}}) - SD(\rho_{\text{NIR and SWIR bands}}) \quad (3)$$

Elevation, slope, and aspect were generated from the SRTM DEM layer, and layerstacked with the seasonal SVIs as the classification feature input for vegetation and land-use mapping.

### 3.2. Image classifier training data

The classification scheme consists of five common forest types in the area, including deciduous, evergreen broadleaf, mixed deciduous and evergreen, conifer, and bamboo, plus three land-use classes: built, agriculture, and bare. A total of 120 single-pixel training samples were extracted and compiled through vegetation type survey and manual image digitization. When available, stable training pixels (Gray & Song, 2013; Shih, Stow, Weeks, & Coulter, 2016) representing a known vegetation or land-use type for the duration of the study period were utilized to classify all four study periods. Through vegetation type survey during Spring 2015, Fall 2015, and Spring 2016 in FNNR, a total of 84 plots that are 20-by-20 m or 30-by-30 m in size were recorded for the five dominant forest types based on accessibility on the ground. These plot locations were cross-referenced with cloud-free Spring Landsat imagery to ensure the forest cover were present in all study periods. Eight out of the 84 forest point samples were found to transition from agriculture to conifer forest between c. 1989 and c. 2016 due to PES implementation. These eight samples were recorded as agriculture class for the first two image dates, and conifer class for the latter two image dates. The remaining 76 samples manifested as stable forest type from the first image date to the last.

For the built, agriculture, and bare land-use classes, a total of 36 stable training pixels were manually selected using the approach similar to that of Stow et al. (2014). The first image date was used as the basis for selecting built training samples. The latter Landsat image dates were used to generate initial agriculture training samples, based on the rationale that agriculture lands were persistent during the study period if afforestation was not observed. The sample pixels were cross-referenced with the 1989 Landsat image date to ensure stability. We also ensured that the training sample pixels were located within a homogeneous portion of the image (i.e. within a single vegetation or land-cover type). The training dataset included 33 samples of mixed forest, 12 broadleaf forest, nine deciduous forest, 10 conifer (18 for 2010 and 2016), 12 bamboo, 15 agriculture (23 for 1989 and 1995), 15 built, and six for bare ground.

### 3.3. Classification, post-processing, and post-classification change analysis

A pixel-based, supervised RF machine learning image classifier was used to generate vegetation and land-use maps for each of the four time periods. The 120 training samples were randomly selected and split into two-thirds and one-third portions respectively for training and testing the image classifier (i.e., cross-validation). A grid search was performed by exhaustively testing combinations of parameters to identify the optimal RF classification parameters—number of trees and number of variables per split. The vegetation and land-use maps were generated with the parameters that yielded the highest testing accuracy. The maps were smoothed with a 3-by-3 pixel majority moving window to minimize mixed-pixel and boundary effects on misclassification, and to generalize to a more realistic minimum mapping unit.

Land-use transition maps were generated through a post-classification comparison approach (Jensen, 1996) to depict afforestation and new built development based on the Landsat-derived vegetation and land-use maps. Logical land change rules were applied such that afforestation activity and new built developments could be mapped with pixels that transitioned from-to classes of interest. To map afforestation activity, pixels that were mapped as agriculture in the earlier study periods and as conifer in the third or fourth study periods were labelled as afforested land. New built development was identified for pixels that were mapped in an earlier image date as any non-built classes (forest, bamboo/conifer, and agriculture) and then as built in a later image date.

### 3.4. Map accuracy assessment

Map accuracy was assessed for the four dates of vegetation and land-use maps, as well as the land-use transition maps. The vegetation and land-use maps were assessed for mapping accuracy using an independent set of 128 accuracy assessment point samples. The samples were created in a random sampling manner with a distance restriction (points to be minimally five Landsat pixels apart), and are well dispersed within the entire mapping area. Samples were labelled manually using the 3 m spatial resolution Planet imagery captured in July 2017 (Planet Team, 2017). These samples represent four vegetation and land-use classes, 32 points per class: forest, agriculture, built, and bamboo/conifer. To keep the analysis consistent, the vegetation and land-use

maps were also categorically aggregated or generalized. The deciduous, evergreen broadleaf, and mixed deciduous and evergreen classes were grouped and recoded as forest; bamboo and conifer classes were merged as a single bamboo/conifer class representing PES afforested lands; agriculture and built remained separate. The accuracy assessment samples were compared to the corresponding image pixels on the generalized maps. Mapping agreement, producer's, user's, and overall accuracies were recorded.

Accuracy of the land-use transition map was assessed in a more qualitative manner due to a lack of available high spatial resolution reference imagery that corresponds to the earlier study periods. Centroids of 24 PES afforested lands were recorded through field visits in FNNR during Spring 2018 and then verified on high spatial resolution satellite imagery on Google Earth. The Landsat-derived afforestation maps were compared to the 24 PES reference points to evaluate the afforestation mapping results. The new built maps were visually inspected in conjunction with high spatial resolution satellite imagery from ArcGIS Basemap, Planet imagery, and Landsat images to identify and label the specific type of land-use changes.

## 4. Results

### 4.1. Vegetation and land-use map accuracy

The four-class vegetation and land-use maps have overall accuracies ranging from 64 to 79% for the four study periods. Table 2 and Table 3 show the accuracy assessment results for before and after PES implementation respectively for the four study periods. The earlier two study periods have moderate mapping accuracies at 64 and 69% for 1989 and 1995 respectively, as shown in Table 2. As seen in Table 3, maps for the latter two (more recent) study periods have higher overall accuracies of 77 and 79% for 2010 and 2016 respectively. Of the four classes, forest and built were consistently classified with high accuracies. Greater mapping confusion occurred for agriculture and bamboo/conifer classes. These land-cover and land-use types are likely under-classified, as indicated by the lower producer's accuracies and higher user's accuracies. The aggregated bamboo/conifer class is often confused with forest, while agriculture is confused with built.

### 4.2. Land change maps and distributions

Afforestation and new built developments were mapped between 1995 and 2010, and 1995–2016. Distributions of afforestation and new built developments were also examined for these two periods. The 1989 date was excluded because of its relatively low agriculture mapping accuracy. Fig. 2 shows afforestation land mapped for 1995–2010. Mapped afforested lands are located mostly near the reserve boundary, particularly alongside river channels, roads, and valleys and creeks that originated from the reserve core. Similar distribution patterns were observed in both 1995–2010 and 1995–2016 afforestation maps. However, the 1995–2016 afforestation map portrays substantial errors in the area to the east of the reserve. This region, approximately 2 $km^2$ in size, remained mostly agriculture from 1995 to 2016, while the 2016 map portrayed it as conifer. This was likely a result of the lower mapping accuracy of bamboo/conifer class, and the under-classification of agriculture from the 2016 image date. In 15 out of the total 24 recorded PES reference locations, afforestation areas are mapped within a three Landsat pixel radius (90 m).

Fig. 3 shows the new developments mapped between 1995 and 2016. Many new built developments are mapped along the reserve boundary and river channels in a linear pattern. In the adjacent reserve environs, new built developments are mostly clustered in nearby towns and villages. While the road networks were mapped more contiguous in 2010 than in 2016, the 2010 map misclassified agriculture land as built in many instances. Indicated by the accuracy assessment result shown in Table 3, the 2010 map likely had an over-classified built class and an under-classified agriculture class that led to more area being mapped as new development in the transition maps.

The new built maps reveal that development in the study area corresponds to widening, paving, and building of roads and freeways, building of tourism and recreational infrastructure, and developing of villages and other infrastructure. Fig. 4 shows examples of the mapped new built developments in detail. Some of the recreational developments that were mapped corresponds to the construction of a golf facility and the station for the gondola lift as seen in Fig. 4a and b respectively, both located on the east side of the reserve. The gondola lift station is slightly larger than one Landsat pixel (30-by-40 m) in size, while the golf course is roughly 0.4 $km^2$ in size. Other mapped infrastructure development primarily corresponds to the following types of construction activities and features: (1) building freeways south and west of reserve as Fig. 4c shows; (2) completion of the road network surrounding the reserve; (3) constructing new roads to connect villages, mostly north and northwest; (4) constructing two dams to the west (Fig. 4d illustrates one of them); (5) developing tourism infrastructures such as reserve entrances on both east and west side of the reserve; and (6) building a sports field at a nearby town to the east.

To improve the reliability of the land transition maps, manual editing was performed to remove the apparent transition errors. Pixel groupings incorrectly classified as new built development due to the misclassified agriculture and built classes were recoded for the new built development maps. Afforested pixels misclassified as agriculture or bamboo/conifer classes were also recoded for the afforestation maps. The areas of afforestation and new developments are summarized based on the mapped and edited land transition maps. Table 4 shows the quantified area of afforestation and new development for 1995–2010 and 1995–2016. Approximately 10 and 12 $km^2$ of the study area was mapped as afforestation based on the 1995–2010 and 1995–2016 land transition maps, respectively. Most of the afforestation activity occurred outside of the reserve, as only 1.33 and 1.45 $km^2$ of afforestation were mapped within the reserve boundary (i.e., core and buffer zones).

A substantial amount of development occurred during the study period based on the new development maps. A total of 25.06 $km^2$ is

**Table 2**
Accuracy assessment results for the c. 1989 and c. 1995 (i.e., prior to PES implementation) classification products generated with the seasonal composite image input and random forest classifier. These values were derived using the final accuracy assessment data on the four-class generalized map. Gray cells indicate agreement.

| Image-derived Class | Reference Class | | | | | | | | User's Accuracy | |
|---|---|---|---|---|---|---|---|---|---|---|
| | Forest | | Agriculture | | Built | | Bamboo & Conifer | | | |
| | 1989 | 1995 | 1989 | 1995 | 1989 | 1995 | 1989 | 1995 | 1989 | 1995 |
| Forest | 28 | 27 | 7 | 6 | 8 | 3 | 10 | 10 | 53% | 59% |
| Agriculture | 1 | 1 | 15 | 18 | 3 | 3 | 3 | 3 | 68% | 72% |
| Built | 0 | 0 | 10 | 6 | 21 | 25 | 1 | 1 | 66% | 78% |
| Bamboo & Conifer | 3 | 4 | 0 | 2 | 0 | 1 | 18 | 18 | 86% | 72% |
| **Producer's Accuracy** | 88% | 84% | 47% | 56% | 66% | 78% | 56% | 56% | Overall Accuracy | |
| | | | | | | | | | 64% | 69% |

**Table 3**
Accuracy assessment results for the c. 2010 and c. 2016 (i.e., post-PES implementation) classification products generated with the seasonal composite image input and random forest classifier. These values were derived using the final accuracy assessment data on the four-class generalized map. Gray cells indicate agreement.

| | Reference Class | | | | | | | | User's Accuracy | |
|---|---|---|---|---|---|---|---|---|---|---|
| | Forest | | Agriculture | | Built | | Bamboo & Conifer | | | |
| Image-derived Class | 2010 | 2016 | 2010 | 2016 | 2010 | 2016 | 2010 | 2016 | 2010 | 2016 |
| Forest | 30 | 29 | 3 | 0 | 0 | 0 | 9 | 10 | 71% | 74% |
| Agriculture | 0 | 0 | 17 | 24 | 2 | 0 | 0 | 3 | 89% | 89% |
| Built | 0 | 0 | 11 | 4 | 30 | 31 | 2 | 2 | 70% | 84% |
| Bamboo & Conifer | 2 | 3 | 1 | 4 | 0 | 1 | 21 | 17 | 88% | 68% |
| **Producer's Accuracy** | 94% | 91% | 53% | 75% | 94% | 97% | 66% | 53% | Overall Accuracy | |
| | | | | | | | | | 77% | 79% |

mapped as new development from 1995 to 2016. Over 37 $km^2$ of the study area was portrayed as new development between 1995 and 2010. Relatively little development occurred within the protected area, as seen in Table 4 and depicted in Fig. 3. Less than 4 $km^2$ are mapped as new built development within the reserve boundary, and less than 0.5 $km^2$ within the core area. Among the observed new built developments within the reserve are small-scale land transitions corresponding to road construction along the valleys on the east and west side, and the recreational/tourism developments (namely reserve entrances, the gondola lift station, and tourism infrastructure at Fanjingshan peak). The majority of the new development is found outside, but adjacent or leading towards the reserve. The golf facility and a tourism attraction of local indigenous tribe were both established within 1 km of the reserve boundary. Over 33 and 23 $km^2$ new development were mapped in the reserve environs for 1995–2010 and.

1995–2016 respectively. Table 4 also reveals that forest was the most common type to transition to built within the reserve area, while agriculture land experienced the most land conversion to built outside of the reserve.

## 5. Discussion

Long-term monitoring of LCLUC in nature reserves is important worldwide given human-induced, widespread degradation of ecosystems (Vitousek, 1994) and associated ecosystem services vital to human being (Daily & Matson, 2008). Such monitoring is also pivotal to assess the efficacy of PES programs in China, which has experienced widespread, PES-related afforestation while subject to relatively rapid infrastructure development at the same time. In this study, we found that the FNNR study area experienced sporadic development and land-use

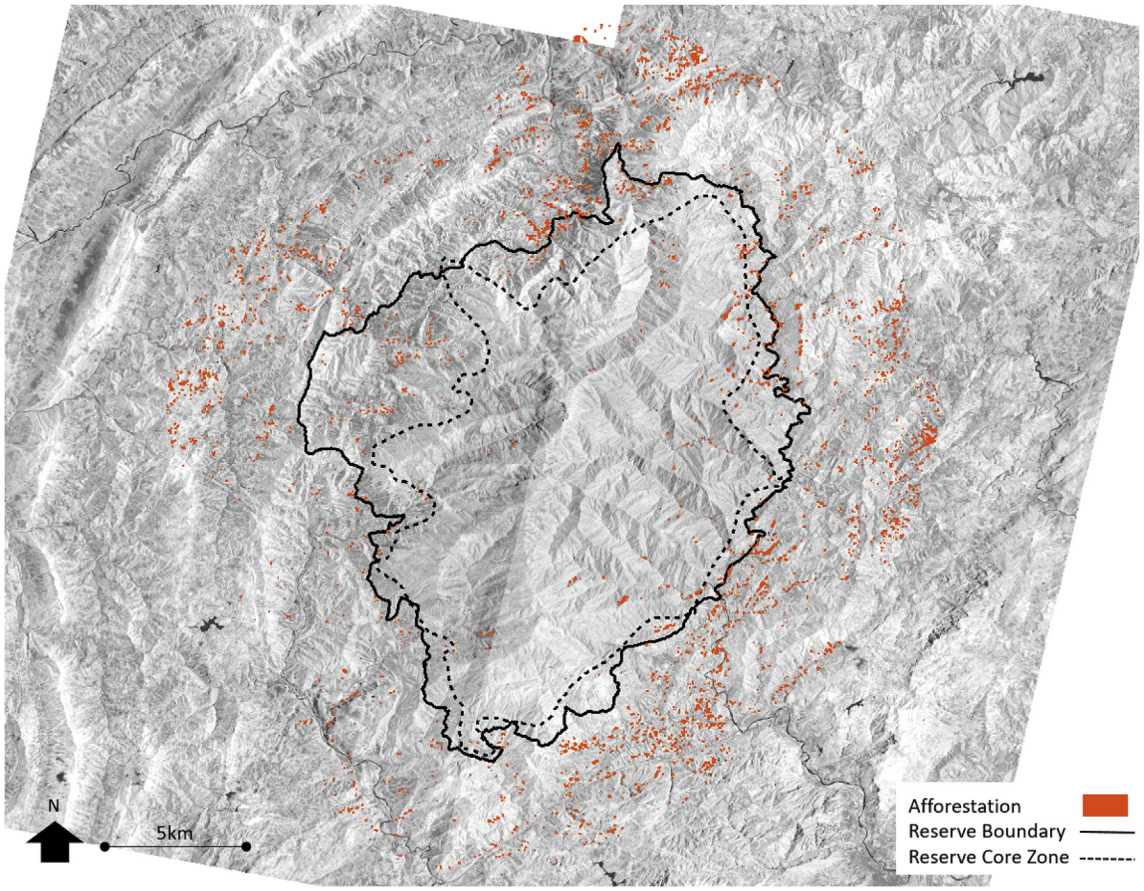


**Fig. 2.** Mapped afforestation from 1995 to 2010 overlaid on a Planet gray-scale NIR image mosaic. Afforestation is mapped from pixels transitioned from agriculture to conifer/bamboo class. The mosaicked Planet image displayed bidirectional effects but remain suitable for visual interpretation.

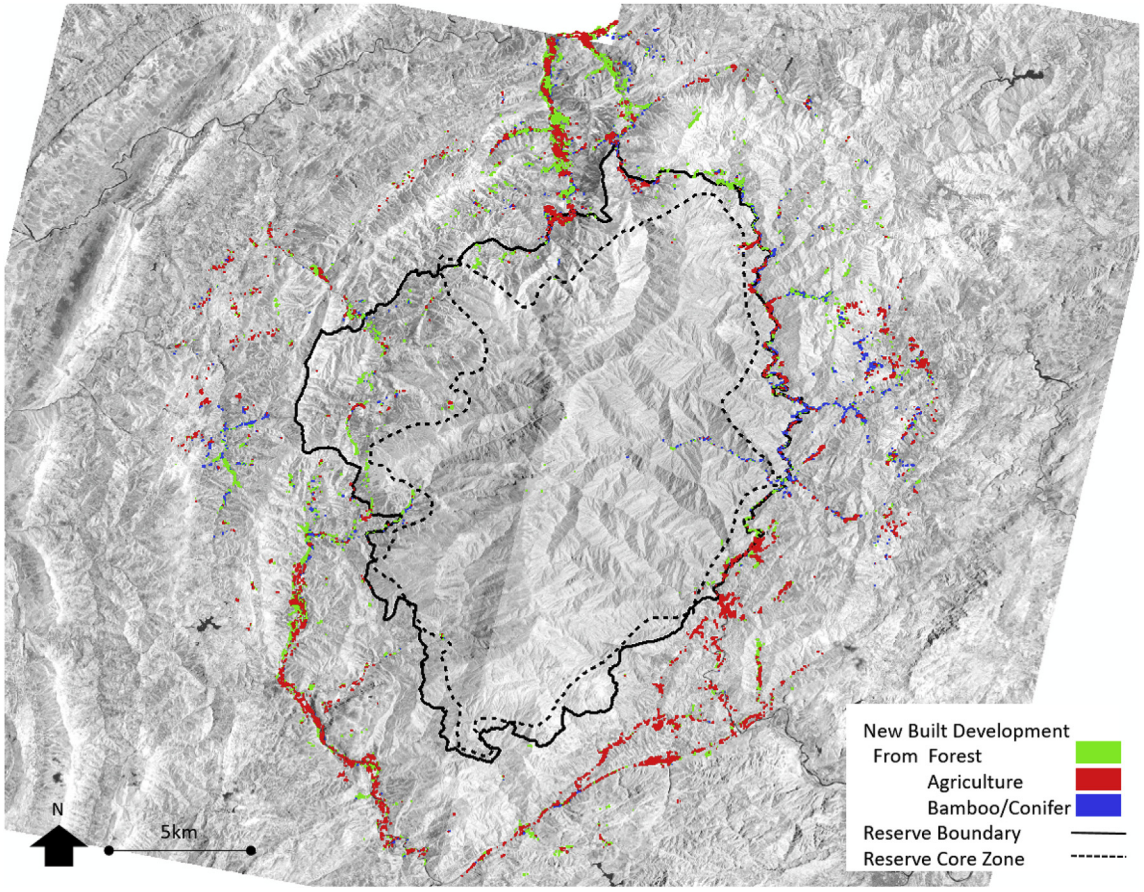


**Fig. 3.** New development map from 1995 to 2016 overlaid on gray-scale NIR Planet image mosaic. New development was identified by pixels transitioned from forest, agriculture, or conifer/bamboo (represented by different colors) to the built class. The mosaicked Planet image displayed bidirectional effects but remain suitable for visual interpretation. (For interpretation of the references to color in this figure legend, the reader is referred to the Web version of this article.)

changes in the core protected area, and more extensive land-use changes in the buffer zone and its adjacent environs between 1995 and 2016 that coincide with the implementation of PES programs.

The quality of the Landsat-derived vegetation and land-use maps and their associated mapping accuracies are generally consistent and suitable for land change monitoring. The c. 2010 and c. 2016 study periods yielded higher classification accuracies compared to the two earlier dates. This could be attributed to the higher quality Landsat images and reference data used for training and accuracy assessment. Seventeen images with acceptable cloud cover were available and incorporated in the seasonal composite for the c. 2016 period, yielding the highest classification accuracy of all four dates. The composites for 2010 and 2016 (later) years are comprised of more summer images that capture the fully leaf-on vegetation signature. For c. 2016, 11 summer images were utilized compared to five for each of the first two dates. The classification training data were derived based on field surveys and images that corresponded more closely with the latter image dates in time. Although training pixels were examined on c. 1989 and c. 1995 Landsat images and evaluated for stability, greater uncertainty exists with over 20 years of temporal difference with the reference data. Generating training data for the RF machine learning image classifier is challenging due to limited access posed by dense vegetation and steep terrain in the study area and lack of available high spatial resolution imagery until after 2010. Thus, training samples are not well-distributed and likely do not encompass the full spectral signature variability of the mapping classes. For future studies, map accuracy could be further evaluated using other techniques more suited for complex and mixed land-cover and land-use products such as fuzzy accuracy assessment (Gopal & Woodcock, 1994).

Most newly developed and many afforestation areas were correctly identified and mapped. However, mapping errors from the earlier two study periods due to the misclassification of agriculture land and conifer/bamboo vegetation are manifested in the afforestation and new built development products. Accurate vegetation and land-use mapping is challenging because of the complex and mixed forest composition and agriculture planting style in this study area. The composition of mixed vegetation cover in the reserve consists of various degrees of conifer, bamboo, evergreen broadleaf, and deciduous forest due to the humid, temperate climate and the steep terrain and elevation gradient. This likely led to the under-classification of conifer and bamboo, and their confusion with the mapped forest class. Bamboo and conifer naturally grow in the region and are often found on the edge of disturbed agriculture land. Agriculture in the FNNR region occurs mostly as small-scale subsistence farming on steep slopes and terraces. Crop types were mostly leafy greens that are small and low in stature, planted sparsely with secondary vegetation mixed in and a lot of soil exposed. The agriculture planting style likely led to a similar spectral signature of high reflective bare or impervious surface especially on the moderate spatial resolution Landsat pixels, and caused the classification confusion with the built class. The farming cycle followed the seasons closely. During winter, agriculture land was mostly bare. This planting pattern is likely why agriculture is sometimes confused with deciduous forest cover.

Open-access and web-based Google Earth Engine software offers a powerful image processing platform. The cloud-computing capability of the Google Earth Engine platform makes it simple and efficient from compositing multi-temporal imagery to implementing machine learning image classification routines to generating results. The coding

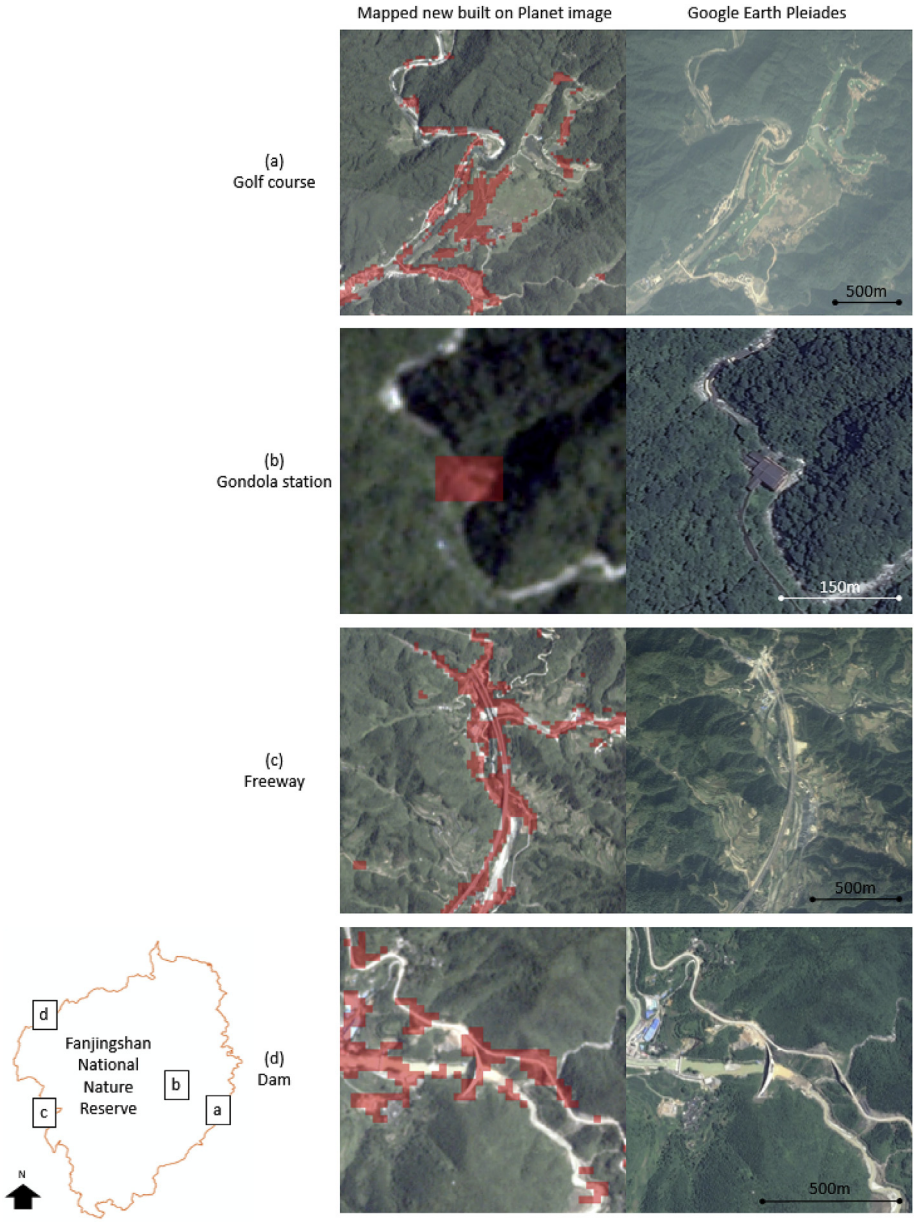


**Fig. 4.** Examples of mapped new built development (shown in red) between 1995 and 2016 overlaid on Planet true-color mosaic image and a Pleiades image from Google Earth: (a) a golf course located to the east of the reserve; (b) a gondola station within the reserve; (c) part of a freeway network to the west of reserve; and (d) a newly-constructed dam also to the west. (For interpretation of the references to color in this figure legend, the reader is referred to the Web version of this article.)

**Table 4**
Mapped new built development and afforestation area for 1995–2010 and 1995–2016 periods. Areas are measured for the FNNR core zone, the entire reserve, and the reserve plus the 6 km surrounding environs. Areas are measured in km$^2$.

| Mapped Area (km$^2$) | Reserve Core | Reserve | Reserve & Environs |
|---|---|---|---|
| 2010 New Built | 0.47 | 3.89 | 37.72 |
| From Forest | 0.30 | 2.08 | 14.18 |
| From Agriculture | 0.05 | 0.94 | 16.11 |
| From Bamboo/Conifer | 0.12 | 0.87 | 7.43 |
| 2010 Afforestation | 0.49 | 1.33 | 10.09 |
| 2016 New Built | 0.25 | 1.90 | 25.06 |
| From Forest | 0.09 | 0.92 | 8.33 |
| From Agriculture | 0.04 | 0.55 | 13.55 |
| From Bamboo/Conifer | 0.12 | 0.42 | 3.18 |
| 2016 Afforestation | 0.16 | 1.45 | 12.46 |

environment allows users to streamline image processing workflow. Its inclusive raster processing functions can be easily implemented using JavaScript, with guidance from documentation and tutorial resources. The platform requires a valid Google user account and a simple online application to access. Compared to many commercial image processing software packages, there is no license or maintenance fees attached to Earth Engine (for education, research, and non-profit users), and it does not require downloading or installing software packages. However, access and performance of Earth Engine is limited when an internet connection is not available or unstable. We found it to be more efficient to view and evaluate results with commercial image processing software (e.g., ERDAS IMAGINE or ArcGIS). Manipulating displays of images and maps is simpler and more efficient when the data are stored locally on the computers. The platform also lacks manual editing capabilities. Regardless, implementing and executing complex image analysis workflows with Google Earth Engine after the methods are tested and documented can be highly automated, as demonstrated in this

study. This is beneficial for reserve by streamlining workflow, minimizing personnel training, and providing an open-access platform that minimizes requirements for costly hardware and software.

We originally attempted to monitor forest cover change as a means of evaluating conservation efforts in FNNR through Landsat-derived canopy fractional cover mapping (CFC; Tsai et al., 2016). Canopy fraction represents the amount of canopy closure as a percentage of each image pixel area occupied by tree canopy (Wang, Qi, & Cochrane, 2005). Continuous CFC data can more precisely represent forest cover variations in complex landscapes (Hansen, 2003), and its magnitude change can reflect the degrees of forest cover change related to degradation, thinning, and clearing. While our results suggested that the modeled CFC changes were likely due to anthropogenic activities, the accuracy of the CFC estimates was uncertain. We derived ground-based estimation of canopy closure through a commonly used digital hemispherical photography technique (DHP; Pueschel, Buddenbaum, & Hill, 2012), and found substantial variability in correspondence between the ground-based and Landsat-derived CFC values, though range and median CFC were similar throughout the areas for which ground-based estimates were made. This could be attributed to the positional uncertainty of ground-based DHP data, and differences in view perspective. The dense canopy in steep terrain likely limited the positional accuracy of the satellite positioning device used to record the DHP data locations. The understory of dense green vegetation provides a low contrasting background, unlike using the up-looking ground-based technique where tree cover contrasts well against a blue sky or cloudy background. We also observed that the majority of land change in FNNR is associated with land use conversion, such as agriculture abandonment, afforestation, and new built expansion, rather than forest thinning and cutting. Mapping multi-temporal vegetation and land-use types was determined suitable for the purpose of environmental monitoring.

It is worth noting that cash crops like tea and fruit trees are also planted as part of the GTGP implementation in FNNR, though limited to several selected villages. Tea bushes planted under the guise of PES were observed in a small village to the northwest of the reserve, on terraces surrounded by conifer stands. We also observed small plots of yellow peaches and pears planted in the southern region, both planted sparsely on terraces and mixed in with secondary regeneration after year 2016. The areas where tea and fruit trees are grown are mapped mostly as agriculture in all four image dates, with some bamboo/conifer cover or mixed forest within. We did not incorporate tea or fruit tree orchards into our classification scheme, as they are not common nor well distributed within the study area.

## 6. Conclusions

Despite the recognized importance of mapping and monitoring vegetation and land-use changes in an era of many global changes arising from or related to rapid population growth, over exploitation of natural resources, and the related environmental degradation (Ripple et al., 2014), this task remains challenging for our cloud-prone and mountainous study area. Our combined techniques of utilizing seasonal image composites, applying illumination normalization, and incorporating ancillary data successfully suppressed terrain effects and minimize persistent cloud cover. The implementation of stable training samples and logical land-use transition rules generated reasonably accurate land-use maps for a period of over 26 years. Future studies could focus on improving the mapping accuracy by increasing the training sample size and increasing the usability of the image processing workflow by integrating the Earth Engine code into a web application with graphical user interface. Yeh (2009) and Feng, Yang, Zhang, Zhang, and Li (2005) indicate that farmers show intentions to return to farming once the PES compensation ends. PES land was also associated with lower wildlife species richness (Chen et al., in review). Our approach and land-use transition maps could provide extensive insight into locations of afforestation and build development lands. More extensive monitoring of land-use conversion is also important for evaluating mid-to long-term ecological impacts of PES and other conservation programs, such as afforestation outcomes, reduced soil erosion, slope stability, and runoff.

## Acknowledgement

This research was funded by the National Science Foundation under the Dynamics of Coupled Natural and Human Systems program [Grant DEB-1212183]. This research also benefited from the Long Gen Ying Travel Grant, Dr. Arthur Getis, and San Diego State University for providing financial and research support.

## References

Aitken, S., An, L., & Yang, S. (2019). Development and sustainable ethics in fanjingshan national nature reserve, China. *Annals of the Association of American Geographers, 109*(2), 661–672.

Belgiu, M., & Drăguţ, L. (2016). Random forest in remote sensing: A review of applications and future directions. *ISPRS Journal of Photogrammetry and Remote Sensing, 114*, 24–31.

Carlson, T. N., & Ripley, D. A. (1997). On the relation between NDVI, fractional vegetation cover, and leaf area index. *Remote Sensing of Environment, 62*(3), 241–252.

Chen, H. L., Lewison, R., An, L., Tsai, Y. H., Stow, D., Shi, L., et al. (in review). Assessing the effects of payment for ecosystem services programs on forest structure and species biodiversity. Ecological Applications.

Coppin, P. R., & Bauer, M. E. (1995). The potential contribution of pixel-based canopy change information to stand-based forest management in the northern U.S. *Journal of Environmental Management, 44*, 69–82.

Coulter, L. L., Stow, D. A., Tsai, Y. H., Ibanez, N., Shih, H. C., Kerr, A., et al. (2016). Classification and assessment of land cover and land use change in southern Ghana using dense stacks of Landsat 7 ETM+ imagery. *Remote Sensing of Environment, 184*, 396–409.

Daily, G. C., & Matson, P. A. (2008). Ecosystem services: From theory to implementation. *Proceedings of the National Academy of Sciences, 105*(28), 9455–9456.

Domaç, A., & Süzen, M. L. (2006). Integration of environmental variables with satellite images in regional scale vegetation classification. *International Journal of Remote Sensing, 27*(7), 1329–1350.

Dorren, L. K., Maier, B., & Seijmonsbergen, A. C. (2003). Improved Landsat-based forest mapping in steep mountainous terrain using object-based classification. *Forest Ecology and Management, 183*(1–3), 31–46.

Farr, T. G., Rosen, P. A., Caro, E., Crippen, R., Duren, R., Hensley, S., et al. (2007). The shuttle radar topography mission. *Reviews of Geophysics, 45*(2).

Feng, Z., Yang, Y., Zhang, Y., Zhang, P., & Li, Y. (2005). Grain-for-green policy and its impacts on grain supply in West China. *Land Use Policy, 22*, 301–312.

Franco-Lopez, H., Ek, A. R., & Bauer, M. E. (2001). Estimation and mapping of forest stand density, volume, and cover type using the k-nearest neighbors method. *Remote Sensing of Environment, 77*(3), 251–274.

Global Environmental Facility Project Team (2004). *The management Plan of Guizhou fanjingshan national nature reserve. Jiangkou.* FNNR GEF Project Management Plan Group.

Gopal, S., & Woodcock, C. (1994). Theory and methods for accuracy assessment of thematic maps using fuzzy sets. *Photogrammetric Engineering & Remote Sensing, 60*(2), 181–188.

Gorelick, N., Hancher, M., Dixon, M., Ilyushchenko, S., Thau, D., & Moore, R. (2017). Google Earth engine: Planetary-scale geospatial analysis for everyone. *Remote Sensing of Environment, 202*, 18–27.

Gray, J., & Song, C. (2013). Consistent classification of image time series with automatic adaptive signature generalization. *Remote Sensing of Environment, 134*, 333–341.

Hall, F., Strebel, D., Nickeson, J., & Goetz, S. (1991). Radiometric rectification: Toward a common radiometric response among multidate, multisensor images. *Remote Sensing of Environment, 35*, 11–27.

Hansen, M. C., DeFries, R. S., Townshend, J. R. G., Carroll, M., Dimiceli, C., & Sohlberg, R. A. (2003). Global percent tree cover at a spatial resolution of 500 meters: First results of the MODIS vegetation continuous fields algorithm. *Earth Interactions, 7*(10), 1–15.

Hansen, M. C., Potapov, P. V., Moore, R., Hancher, M., Turubanova, S., Tyukavina, A., et al. (2013). High-resolution global maps of 21st-century forest cover change. *Science, 342*(6160), 850–853.

Harkness, J. (1998). Recent trends in forestry and conservation of biodiversity in China. *The China Quarterly, 156*, 911–934.

Jensen, J. R. (1996). *Introductory digital image processing: A remote sensing perspective.* Saddle River, New Jersey: Prentice-Hall.

Johansen, K., Phinn, S., & Taylor, M. (2015). Mapping woody vegetation clearing in queensland, Australia from Landsat imagery using the Google Earth engine. *Remote Sensing Applications: Society and Environment, 1*, 36–49.

Kotsiantis, S. B., Zaharakis, I., & Pintelas, P. (2007). Supervised machine learning: A review of classification techniques. *Emerging artificial intelligence applications in computer engineering, 160*, 3–24.

Liu, J., Linderman, M., Ouyang, Z., An, L., Yang, J., & Zhang, H. (2001). Ecological degradation in protected areas: The case of wolong nature reserve for giant pandas.

*Science, 292*(5514), 98–101.
Liu, J., Li, S., Ouyang, Z., Tam, C., & Chen, X. (2008). Ecological and socioeconomic effects of China's policies for ecosystem services. *Proceedings of the National Academy of Sciences, 105*(28), 9477–9482.
Liu, L., Tang, H., Caccetta, P., Lehmann, E. A., Hu, Y., & Wu, X. (2013). Mapping afforestation and deforestation from 1974 to 2012 using Landsat time-series stacks in Yulin District, a key region of the Three-North Shelter region, China. *Environmental Monitoring and Assessment, 185*(12), 9949–9965.
Masek, J. G., Vermote, E. F., Saleous, N. E., Wolfe, R., Hall, F. G., Huemmrich, K. F., et al. (2006). A Landsat surface reflectance dataset for North America, 1990-2000. *IEEE Geoscience and Remote Sensing Letters, 3*(1), 68–72.
Moran, M. S., Jackson, R. D., Slater, P. N., & Teillet, P. M. (1992). Evaluation of simplified procedures for retrieval of land surface reflectance factors from satellite sensor output. *Remote Sensing of Environment, 41*, 169–184.
Myers, N., Mittermeier, R. A., Mittermeier, C. G., Da Fonseca, G. A., & Kent, J. (2000). Biodiversity hotspots for conservation priorities. *Nature, 403*(6772), 853.
Park, A. B., Houghton, R. A., Hicks, G. M., & Peterson, C. J. (1983). Multitemporal change detection techniques for the identification and monitoring of forest disturbances. *Proceedings 17th international symposium on remote sensing of environment* (pp. 77–97). Ann Arbor, MI.
Planet Team (2017). *Planet application program interface: In space for life on Earth.* San Francisco, CA. URL https://api.planet.com.
Pueschel, P., Buddenbaum, H., & Hill, J. (2012). An efficient approach to standardizing the processing of hemispherical images for the estimation of forest structural attributes. *Agricultural and Forest Meteorology, 160*, 1–13.
Qi, J., Chehbouni, A., Huete, A. R., Kerr, Y. H., & Sorooshian, S. (1994). A modified soil adjusted vegetation index. *Remote Sensing of Environment, 48*(2), 119–126.
Ripple, W. J., Estes, J. A., Beschta, R. L., Wilmers, C. C., Ritchie, E. G., Hebblewhite, M., et al. (2014). Status and ecological effects of the world's largest carnivores. *Science, 343*(6167).
Rodriguez-Galiano, V. F., Ghimire, B., Rogan, J., Chica-Olmo, M., & Rigol-Sanchez, J. P. (2012). An assessment of the effectiveness of a random forest classifier for land-cover classification. *ISPRS Journal of Photogrammetry and Remote Sensing, 67*, 93–104.
Schneider, A. (2012). Monitoring land cover change in urban and peri-urban areas using dense time stacks of Landsat satellite data and a data mining approach. *Remote Sensing of Environment, 124*, 689–704.
Shih, H. C., Stow, D. A., Weeks, J. R., & Coulter, L. L. (2016). Determining the type and starting time of land cover and land use change in southern Ghana based on discrete analysis of dense Landsat image time series. *IEEE Journal of Selected Topics in Applied Earth Observations and Remote Sensing, 9*(5), 2064–2073.
Stow, D. A., Shih, H. C., & Coulter, L. L. (2014). Discrete classification approach to land cover and land use change identification based on Landsat image time sequences. *Remote sensing letters, 5*(10), 922–931.
Tsai, Y. H., Stow, D., Chen, H. L., Lewison, R., An, L., & Shi, L. (2018). Mapping vegetation and land use types in fanjingshan national nature reserve using Google Earth engine. *Remote Sensing, 10*(6), 927.
Tsai, Y. H., Stow, D., Shi, L., Lewison, R., & An, L. (2016). Quantifying canopy fractional cover and change in Fanjingshan National Nature Reserve, China using multi-temporal Landsat imagery. *Remote Sensing Letters, 7*(7), 671–680.
Uchida, E., Xu, J., & Rozelle, S. (2005). Grain for green: Cost-effectiveness and sustainability of China's conservation set-aside program. *Land Economics, 81*(2), 247–264.
Vermote, E., Justice, C., Claverie, M., & Franch, B. (2016). Preliminary analysis of the performance of the Landsat 8/OLI land surface reflectance product. *Remote Sensing of Environment, 185*, 46–56.
Vitousek, P. M. (1994). Beyond global warming: Ecology and global change. *Ecology, 75*(7), 861–1876.
Wandersee, S. M. (2013). *Land-cover and land-use change in human-environment systems: Understanding complex interactions among policy and management, livelihoods, and conservation.* Santa Barbara: Doctoral dissertation, University of California.
Wang, C., Qi, J., & Cochrane, M. (2005). Assessment of tropical forest degradation with canopy fractional cover from Landsat ETM+ and IKONOS imagery. *Earth Interactions, 9*(22), 1–18.
Wu, C. (2004). Normalized spectral mixture analysis for monitoring urban composition using ETM+ imagery. *Remote Sensing of Environment, 93*(4), 480–492.
Xie, Y., Sha, Z., & Yu, M. (2008). Remote sensing imagery in vegetation mapping: A review. *Journal of Plant Ecology, 1*(1), 9–23.
Xu, J., Tao, R., Xu, Z., & Bennett, M. T. (2010). China's sloping land conversion program: Does expansion equal success? *Land Economics, 86*(2), 219–244.
Yang, Y. Q., Lei, X. P., & Yang, C. D. (2002). *Fanjingshan research: Ecology of the wild Guizhou snub-nosed monkey (rhinopithecus bieti).* Guiyang: Guizhou Science Press.
Yeh, E. T. (2009). Greening western China: A critical view. *Geoforum, 40*, 884–894.
Yuan, F., Sawaya, K. E., Loeffelholz, B. C., & Bauer, M. E. (2005). Land cover classification and change analysis of the Twin Cities (Minnesota) Metropolitan Area by multitemporal Landsat remote sensing. *Remote Sensing of Environment, 98*(2–3), 317–328.
Zhou, H., & Van Rompaey, A. (2009). Detecting the impact of the “Grain for Green” program on the mean annual vegetation cover in the Shaanxi province, China using SPOT-VGT NDVI data. *Land Use Policy, 26*(4), 954–960.
Zhou, D., Zhao, S., & Zhu, C. (2012). The grain for green Project induced land cover change in the Loess Plateau: A case study with ansai county, shanxi province, China. *Ecological Indicators, 23*, 88–94.